1 **Uncertainty in counting ice nucleating particles with continuous**

2 **flow diffusion chambers**

3 **Sarvesh Garimella[1], Daniel A. Rothenberg[1], Martin J. Wolf[1], Robert O. David[2], Zamin A.**

4 **Kanji[2], Chien Wang[1], Michael Rösch[1], and Daniel J. Cziczo[1,3]**

5 [1] {Department of Earth, Atmospheric and Planetary Sciences, Massachusetts Institute of

6 Technology, Cambridge, MA, United States}

7 [2] {Institute for Atmospheric and Climate Science, ETH Zurich, Zurich, Switzerland}

8 [3] {Department of Civil and Environmental Engineering, Massachusetts Institute of

9 Technology, Cambridge, MA, United States}

11 Correspondence to: D. J. Cziczo (djcziczo@mit.edu)

1 **Abstract**

2 This study investigates the measurement of ice nucleating particle (INP) concentration and sizing

3 of crystals using continuous flow diffusion chambers (CFDCs). CFDCs have been deployed for

4 decades to measure the formation of INPs under controlled humidity and temperature conditions

5 in laboratory studies and by ambient aerosol populations. These measurements have, in turn,

6 been used to construct parameterizations for use in models by relating the formation of ice

7 crystals to state variables such as temperature, humidity, and aerosol particle properties such as

8 composition and number. We show here that assumptions of ideal instrument behavior are not

9 supported by measurements made with a commercially available CFDC, the SPectrometer for

10 Ice Nucleation (SPIN), and the instrument on which it is based, the Zurich Ice Nucleation

11 Chamber (ZINC). Non-ideal instrument behavior, which is likely inherent to varying degrees in

12 all CFDCs, is caused by exposure of particles to different humidities and/or temperatures than

13 predicated from instrument theory of operation. This can result in a systematic, and variable,

14 underestimation of reported INP concentrations. We find here variable correction factors from

15 1.5-9.5, consistent with previous literature values. We use a machine learning approach to show

16 that non-ideality is most likely due to small scale flow features where the aerosols are combined

17 with sheath flows. Machine learning is also used to minimize the uncertainty in measured INP

18 concentrations. We suggest that detailed measurement, on an instrument-by-instrument basis, be

19 performed to characterize this uncertainty.

1. Introduction

Aerosol particles affect the climate system via their ability to interact with radiation and act as the sites upon which water condenses to form liquid and ice clouds (Pruppacher and Klett, 1997; Seinfeld and Pandis, 2006; Boucher et al., 2013). Those that facilitate ice crystal formation above the temperature or below the humidity of homogeneous freezing are called ice nucleating particles (INPs) and these affect the formation and persistence of mixed-phase and cirrus clouds (Forster et al., 2007). The interactions between INPs and cold clouds are a measurement challenge because such clouds occur either high in the atmosphere or near the poles and are difficult to access (Rossow and Schiffer, 1999). Continuous flow diffusion chambers (CFDCs) have provided a means to understand ice cloud formation by measuring INP concentrations in the field. By exposing an ambient aerosol population to controlled humidity and temperature conditions, the ability of natural aerosols to act as INPs can be quantified (DeMott et al., 2003a; DeMott et al., 2003b; Chou et al., 2011; Boose et al., 2016).

Measurements of INP concentration using CFDCs have been used to construct model parameterizations that relate the formation of ice crystals to temperature and aerosol particle number and size (DeMott et al., 2010; Tobo et al, 2013; DeMott et al., 2015). Using such parameterizations, global aerosol transport models attempt to link aerosol emissions to their potential to impact ice cloud formation and thus climate (Vergara-Temprado et al., 2016). The use of CFDC data for parameterization of ice formation in such models highlights the need for assessing the accuracy and bias of such measurements.

CFDC instruments are able to determine INP concentration by drawing in aerosol particles and controlling the temperature and relative humidity to which they are exposed (Rogers, 1988; Stetzer et al., 2008; Garimella et al., 2016). Although there are instrument-to-instrument

1   differences in geometry and flows, typically particles are drawn through an inlet and contained

2   between two sheath flows (Figure 1). These three flows pass between two ice-coated walls that

3   are held at different, sub-0º C temperatures. Water vapor and heat diffuse from the warm wall to

4   the cold wall, such that approximately linear gradients of both quantities exist across the width of

5   the chamber. Because the saturation vapor pressure exhibits a nonlinear temperature dependence,

6   the air within the chamber is supersaturated with respect to ice. The variation in heat and vapor

7   diffusion results in a maximum in supersaturation near the center of the chamber (Rogers, 1988).

8   Particles constrained to a narrow central lamina by the sheath flows should, in theory, be

9   exposed to only the maximum saturation with a small uncertainty in temperature and humidity.

10   The fractional width of the lamina is typically taken to be the ratio of the incoming aerosol flow

11   rate to the total (sample + sheaths) flow rate through the chamber (Rogers, 1988).

12   A sufficiently large temperature gradient between the walls can cause lamina conditions to

13   not only exceed ice but also liquid water saturation (Rogers, 1988; Stetzer et al., 2008; Garimella

14   et al., 2016). Droplet formation is important since many CFDCs measure only the size of objects

15   exiting the chamber with an Optical Particle Counter (OPC, Rogers, 1988; DeMott et al., 2015).

16   The presence of droplets can therefore be misinterpreted as a higher abundance of ice crystals.

17   The impact of droplet formation is minimized by the utilization of an "evaporation region" in

18   most modern CFDCs. These regions are isothermal and ice-coated sections at the bottom of the

19   chamber where small droplets are evaporated by subsaturated conditions with respect to liquid

20   water. Nonetheless, a CFDC run with a sufficiently large temperature gradient between the walls

21   can create droplets large enough to survive evaporation sections. This condition is known as

22   "droplet breakthrough" and is specific to each CFDC's geometry and flow characteristics

23   (Rogers, 1988; Stetzer et al., 2008; Garimella et al., 2016).

1   Instruments rarely follow theoretical predictions. In the case of CFDCs, this is often due to

2   non-ideal flow and deviations from isothermal conditions. DeMott et al. (2015) discussed the

3   effect of aerosol "spreading" outside the lamina as well as other possible factors that, in

4   combination, could contribute to a low bias in the number of INP measured. Here, we extend the

5   work of DeMott et al. (2015) with a quantitative analysis of the source and effect of spreading

6   and discussion of the impact on CFDC data. For this work we use the Zurich Ice Nucleation

7   Chamber (ZINC, Stetzer et al., 2008) and the commercial version, the SPectrometer for Ice

8   Nucleation (SPIN, Garimella et al., 2016). We specifically considered effects in the regime

9   supersaturated with respect to liquid water (immersion freezing) but believe these results are also

10   applicable in the sub-saturated regime (depositional nucleation). The automation of these

11   instruments, in particular the large amount of "housekeeping" data autonomously recorded to

12   characterize SPIN instrument behavior, makes these chambers suitable for exploring this effect.

13   We apply a machine learning algorithm for analysis in order to process the large amount of data

14   and generate statistical inferences to constrain the spreading effect. We suggest the spreading

15   effect can be best visualized as a deviation from laminar flow and non-isokinetic injection as the

16   particles are drawn into the chamber. We conclude that the non-ideal conditions are likely

17   universal but also dependent on the geometry and flow characteristics of each CFDC chamber.

19   **2. Methodology**

20   **2.1 Particle timing tests**

21   The ZINC and SPIN CFDCs have been described in detail previously (Stetzer et al., 2008;

22   Garimella et al., 2016). To measure the degree of particle spreading outside the lamina a precise

23   particle pulse was introduced into the chambers. In the case of SPIN this was a 1 second pulse

1   while for ZINC a ~10 second pulse was used with automated and manual valves, respectively. In

2   both cases, a valve at the chamber inlet was used to control the pulse. Under ideal conditions,

3   regardless of duration, this should correspond to an equivalent particle pulse at the chamber

4   outlet. Non-idealities have been shown to lead to particle spreading across the width of the

5   chamber as they traverse its length by DeMott et al. (2015). For this work, the arrival of particles

6   was measured at the chamber outlet with a Condensation Particle Counter (CPC, Brechtel, Inc.

7   Model (BMI) 1720 for SPIN, and TSI CPC 3772/3787 for ZINC). A wider particle pulse (in

8   time) measured at the outlet indicates more spreading of the particles across the width of the

9   chamber, since the fastest particles travel closer to the center of the chamber under a laminar

10   flow assumption. This is shown in Figure 2 for ZINC experiments at a total flow rate of 10 lpm

11   and chamber conditions of -40º C and 102% relative humidity (RH, Panel A) and 110% RH with

12   respect to water (Panel B). This temperature was used to determine variation of particle loss with

13   respect to temperature from the lamina and because it is in the homogeneous freezing regime

14   where all test particles should be able to nucleate ice. At this lamina temperature the difference

15   between the wall temperatures is larger for a given supersaturation than at a higher temperature

16   and this maximized any resulting turbulence effect on particle migration from the lamina. 10-

17   second pulses were produced with 200 nm ammonium nitrate (Sigma Aldrich) particles which

18   were wet-generated using an atomizer and size selected with a differential mobility analyzer (TSI

19   DMA 3082). CPC measurement at the input (CPC_{in}) verifies production of a ~10-second pulse

20   while the output particles (CPC_{out}) continue for 20 – 30 seconds.

21   The SPIN data exhibit the same behavior. SPIN particle distributions were measured for 25

22   1-second aerosol pulses at constant isothermal conditions of 20° C and ~10 lpm flow. 100 nm

23   diameter ammonium sulfate particles wet-generated and dried with a BMI 9203 Aerosol

1 Generator and mobility diameter selected with a BMI Differential Mobility Analyzer Model

2 2100 were used. Combining information from a measured particle pulse and a calculated velocity

3 profile, the corresponding distribution of particles across the width of the chamber for that

4 particular pulse can be inferred (Figure 3). Buoyancy effects on mean chamber flow and mean

5 particle position are accounted for in the calculation of the velocity profiles (Rogers, 1988). The

6 particle distributions are reconstructed by assigning the first detected particles to the maximum

7 velocity position in the calculated flow profile and the assigning peak particle concentration to

8 the calculated lamina position (about which spreading occurs). The particles in the tail of the

9 pulse are assigned positions corresponding to their relative velocities, which are derived from

10 their relative arrival times.

11 A further ~250 pulse measurements using polydisperse ambient aerosol particles were

12 conducted using the SPIN setup at Storm Peak Laboratory (Steamboat Springs, Colorado, 3220

13 m M.S.L.; 40.455ºN, -106.744ºW) to capture the spreading effect variability in an environment

14 where INP field measurement campaigns occur (DeMott et al., 2003a). These tests were across a

15 range of chamber thermodynamic conditions (lamina humidities between ice and water

16 saturation at temperatures -15 to -40º C). We note that diffusive and other forces may differ

17 across particle sizes. Monodisperse particles were tested under laboratory and polydisperse

18 particles under field conditions; future studies may consider a full range of particle sizes

19 applicable to particular CFDCs.

21 **2.2 Machine learning prediction**

22 A random forest regression (RFR) (Breiman, 2001) was used to predict the fraction of

23 particles that remained in the aerosol lamina (hereafter "f_{lam}"). In this application RFR is

1   similar to a multiple linear regression except that it grows a forest of bootstrap aggregated (or

2   "bagged") decision trees to fit the data instead of using a linear model. Bootstrap aggregation

3   avoids overfitting the data, provides uncertainty quantification for each prediction using the out-

4   of-bag (oob) prediction error, ranks the variables by their importance by comparing oob

5   prediction errors, and does not assume linear relationships between variables (Breiman, 2001).

6   First, the complete set of housekeeping variables recorded for SPIN is input into the RFR, for

7   which they are termed "features". This housekeeping data set is normally recorded to verify

8   instrument operation and no *a priori* assumptions are made as to which variables are the most

9   important predictor of f_{lam}. The RFR indicates the most important predictors by comparison to

10   the experimental pulse results. As an example, ambient temperature might not be expected to be

11   an important factor in the spreading effect but it was not removed from the data set; that decision

12   was left to the RFR. Feature importance was observed to fall exponentially and those within the

13   first two e-folding lengths of importance were maintained in a reduced RFR model. The reduced

14   RFR subset included 65 variables including wall temperature, flows, and saturation conditions

15   predominantly in the middle and top sections of the SPIN chamber (Garimella et al., 2016); this

16   is the region of the chamber where aerosol is initially encased within the sheath flows. This

17   suggests that turbulence or other small-scale flow features in this region are responsible for the

18   spreading effect in the region where the particle flow is injected into the chamber. However, we

19   can not preclude that other processes taking place in this region, such as thermophoresis, are not

20   also partially responsible. The top ten most important features are listed in Table 1.

22   **3. Results and Discussion**

1   Figure 4 shows the results from the 25 particle timing tests at 20° C and ~10 lpm flow

2   conditions. Wall temperatures remained within ± 1 degree of the set point for all experiments.

3   The fraction of particles that remained in the aerosol lamina varied despite constant flow, aerosol

4   properties, and temperature. Figure 5 shows the results from 267 ambient particle pulse

5   experiments in the aforementioned temperature and saturation range. In Figure 5, f_{lam} is plotted

6   against the lamina temperature and ice saturation ratio (S_{ice}) calculated for walls at ice saturation

7   and with temperatures corresponding to the measurement average value (Garimella et al., 2016).

8   Data are not highly correlated to either. The mean and standard deviation of f_{lam} are 0.25 ± 0.14

9   and, depending on the specific conditions, the distribution exhibits values that vary between 0.03

10   and 0.7 (i.e., between 3 and 70% of particles were within the lamina).

11   The reduced RFR described in Section 2.2 can be used to predict f_{lam} (mean values and

12   standard deviations) based on the SPIN variables shown to be most important. Figure 6 shows

13   the performance of this approach, which has an oob mean squared prediction error of 0.008

14   whereas simply selecting the mean value for f_{lam} from the distribution in Figure 5 results in a

15   mean squared error for predicting f_{lam} of ~0.02. Thus, the RFR approach reduces the

16   uncertainty by ~60%.

17   DeMott et al. (2015) noted the non-ideality, including due to particles spreading beyond the

18   lamina, in the Colorado State University CFDC chamber. They proposed the use of a "calibration

19   factor" (cf) = 3 by which the measured INP number could be multiplied to provide a corrected

20   value. Previous studies, including Tobo et al. (2013), used $cf = 1$; this corresponds to an

21   assumption that all particles in a CFDC exist within the lamina. It should be noted particle

22   properties, such as size, shape and hygroscopicity may have an effect on the *cf* and that the value

23   found by DeMott et al. (2015) may not be universal even for that CFDC. The value of *cf* = 3

1 does correspond to a constant 33% of particles existing within the lamina, regardless of flow or

2 thermodynamic state, for those experiments. The distribution found here corresponds to a

3 variable correction factor in the range of $cf = 1.4$ to 9.5, depending on the experiment, with a

4 mean of 4. We note the $cf = 3$ value reported by DeMott et al. (2015) is for a different CFDC

5 but falls within the range measured here. This suggests that cf could depend on various

6 instrument control factors and would require RFR analysis for the various CFDC configurations

7 to predict cf.

8   Further evidence to support the spreading effect is provided by the size of the ice crystals

9 measured at the output of a CFDC. Theoretically, a monodisperse population of an aerosol

10 composition that only nucleates ice homogeneously should exhibit freezing almost at the same

11 time and location within a CFDC chamber. This is because particles should equilibrate with the

12 internal chamber conditions within ~1 second of entering the chamber and then freeze rapidly

13 due to the resulting nucleation rate at these conditions (Koop et al., 2000). This should translate

14 to a quasi-monodisperse ice crystal size distribution at the chamber output. The size of the ice

15 crystals should be a function of the chamber RH and temperature and equivalent to the amount of

16 vapor-deposited water under these conditions. Therefore, differences in ice crystal size should

17 primarily be due to particles that leave the lamina and experience varying supersaturations and

18 residence times in the chamber. The result of the extended time it takes for particles to exit the

19 chamber due to spreading would be (1) larger crystals due to extended time in a supersaturated

20 region and (2) a broadening of the ice crystal size distribution due to residence time and

21 supersaturation variability the particles are exposed to. Experiments run with the ZINC chamber

22 confirm a non-monodisperse ice crystal size distribution (Figure 7).

1   In order to consider the effect of spreading beyond the lamina, aerosol particles were

2   assumed to nucleate ice upon entering the chamber since the -40° C lamina temperature was

3   below that required for homogeneous ice nucleation. We note there is a short delay not directly

4   accounted for in this calculation for thermal equilibration (~ 0.1 – 0.8 seconds at -40 °C

5   assuming heat transfer coefficients for the NH_4NO_3 particles) and ~1.0 second for the particles

6   to travel to the ice coated region of the chamber (Stetzer et al., 2008). The combination of

7   velocity profile and residence time from the pulse experiments (Figure 2) were then used to

8   determine the location of the particles in the lamina and therefore the time they were exposed to

9   variable supersaturation and the subsequent size to which they would grow.

10   The baseline crystal size was when all particles remained within the predicted lamina (i.e.,

11   within the dashed lines in Figure 2). Ice crystal size was calculated per the formulation of Rogers

12   and Yau, 1989. Crystals were assumed to be spherical due to the ice forming homogeneously

13   from sub-micrometer diameter particles (Järvinen et al., 2016). The initial ice crystal size was

14   assumed to be that of ammonium nitrate at the initial dry diameter, which may be a slight

15   underestimation due to hygroscopic growth before freezing occurred. However, calculations with

16   a doubling of the initial particle size had minimal impact on the final ice crystal size so this

17   assumption was maintained for all calculations. An accommodation coefficient of 0.2 (Skrotzki

18   et al., 2013) and the calculated residence time in the lamina (~10 seconds) were used to predict

19   the ice crystal sizes. The calculations resulted in monodisperse ice crystals at ~4 micrometers

20   diameter (Figure 7, red histogram).

21   If minor spreading in time with respect to that predicted when particles remain in the lamina

22   is allowed at the level of +/- 1 second, the ice crystal size distribution broadened (3-4

23   micrometers diameter; Figure 7, purple histogram). The extended time that ice crystals were

1   observed to remain in ZINC experiments (Figure 2) caused a further broadening in ice crystal

2   size distribution (3-7 micrometers diameter; Figure 7, yellow histogram). The measured ice

3   crystal size distribution (Figure 7, blue histogram) shows particles predominantly from 2-7

4   micrometers and is most consistent with the calculations made for ice crystal growth that include

5   the spreading effect. It is important to note that the previous calculations are from a simple ice

6   growth model and are used to illustrate that observed ice crystal size distributions are also

7   consistent with particles spreading beyond the lamina. In addition to spreading, there are other

8   reasons that ice crystals smaller than the theoretical size might exist. These include uncertainty in

9   shape, refractive index and crystals that are undersized by passing through the edge of the ZINC

10   OPC (Stetzer et al., 2008). Furthermore, literature values of accommodation coefficient ranges

11   between 0.2 and 1 (e.g., Skrotzki et al., 2013). Here, 0.2 was used for these calculations. A value

12   of 0.1 would result in ~10% smaller ice crystals, which is still not sufficient to fully account for

13   the ice crystals < 2 micrometers diameter observed in the OPC.

14   The effect of particle spreading outside the lamina on CFDC reports of INP concentration

15   measurements can be visualized using the data collected here. Figure 8 shows idealized

16   activation curves (i.e., nucleation of ice or droplets) at various f_{lam} values. Note that f_{lam} and cf

17   can be thought of interchangeably where 33% and 3 are, respectively, (inversely) equivalent. In

18   Figure 8, the aerosol population is assumed to be idealized "perfect" immersion mode INPs that

19   form ice crystals immediately upon exposure at water saturation (S_{liq}=1); this could be viewed

20   as a laboratory test of effective immersion INPs. In the case where the CFDC is assumed to

21   operate ideally, all particles are constrained within the lamina ($f_{lam} = 100\%$) and all nucleation

22   occurs at S_{liq}=1 (solid line). The other three curves in Figure 8 correspond to increasingly less

23   ideal behavior (i.e., increasingly fewer particles in the lamina), corresponding to f_{lam} falling

1 from 33 to 10%. The deviation from the ideal case can be viewed as a higher than saturation

2 condition required at the centerline so the particle farthest outside the lamina experiences this

3 value. These curves can also be interpreted as cases where cf is fixed but increases from 3, the

4 value suggested by DeMott et al. (2015), to 10, the worst case found in this work.

5   Homogeneous freezing experiments conducted in ZINC with 400 nm dry diameter NH_4NO_3

6 particles (see Figure 9) demonstrate that $S_{liq} > 0.99$ (as predicted by Koop et al. (2000)) is

7 required for all particles to freeze at -40° C, even after accounting for uncertainties in S_{liq} (Figure

8 9, shown in blue shading), of the lamina. Furthermore, within this uncertainty, ~ 70% of the

9 particles freeze in ZINC, consistent with the pulse tests in shown in Figure 2 if counting

10 uncertainties of ~14% arising from the CPC and OPC are considered. Indeed, to observe 100%

11 of particles freezing, $S_{liq} = 1.05$ must be reached in ZINC, suggesting that ~30% of the particles

12 escape the lamina even in the best observed case presented in this work. In the example of Figure

13 9, quoting an active fraction at a specific $S_{liq} < 1.05$ would result in underestimating this value as

14 we know in an ideal case (no lamina spreading) the active fraction should be unity at $S_{liq} = 1$.

15   Figure 10 expands on Figure 8 by considering another idealized case, but one more

16 applicable to measurement of an ambient aerosol population. In this case only 10% of the

17 particles are perfect immersion mode INP, whereas the rest are cloud condensation nuclei (CCN)

18 that activate at exactly $S_{liq} = 1$. The evaporation section on the bottom of the heuristic chamber

19 causes droplets to evaporate until breakthrough at $S_{liq} > 1.07$ (Garimella et al., 2016). In the

20 ideal case all particles are constrained within the lamina and 10% of particles nucleate ice at a

21 CFDC saturation of $S_{liq} = 1$ (panel a, solid black line). The remaining 90% of particles break

22 through as droplets at $S_{liq} > 1.07$ (panel a, solid blue line). The other three curves correspond to

23 the increasingly less ideal behavior presented in Figure 8, corresponding to f_{lam} falling from 33

to 10%. In these cases an increasingly higher maximum saturation is required so that the particles farthest from the centerline experience $S_{liq} = 1$ (ice nucleation) and 1.07 (droplet breakthrough). The resulting activation curves of droplets and ice crystals are indistinguishable (i.e., a composite of the red and blue traces in panel a), historically the case for CFDC detectors (Rodgers, 1988), as shown in panel b. We propose the shape of the idealized activation curve in Figure 10b resembles that of experimental CFDC activation curves (DeMott et al., 2015) due to the primary importance of the particle spreading effect.

4. Conclusions

The results presented here indicate that neither the reported thermodynamic conditions nor results from a single timing test capture the full variability of f_{lam} in the SPIN CFDC. Following on the results of DeMott et al. (2015), the findings in this study indicate that f_{lam} is not unity in real CFDCs. We show that it is also variable in ZINC and SPIN. We believe this is likely universal to all CFDC instruments although the degree of uncertainty and magnitude of the effect are probably a function of instrument geometry (i.e., parallel plate, cylindrical, etc.), flow and thermodynamic conditions. The non-uniform time particles spend in a CFDC has complex results on ice nucleation and crystal growth, including larger and broader size distributions than predicted by theory.

A machine learning approach used housekeeping data to show that the most likely reason for the lack of ideality is small scale flow features near the inlet of the chamber where the aerosol sample flow is sheathed. The RFR deemed variables including wall temperature, flows, and thermodynamic variables predominantly in the middle to top section of the SPIN chamber (i.e., at the injection point) as most important. Moreover, the RFR approach was able to better predict

1   f_{lam}, and therefore the conditions experienced by the aerosols in the chamber than standard

2   CFDC flow theory with an overall reduction in uncertainty by $\sim 60\%$.

3   Finally, we show the particle spreading effect explains why CFDC chambers are often

4   operated at non-physical S_{liq} values to measure immersion mode INP number concentration and

5   why the reported numbers are strongly dependent on S_{liq}. Theoretically, immersion mode

6   nucleation should occur at $S_{liq} = 1$, yet reports with CFDCs often show increased

7   concentrations up to, and often well beyond, 1.05. By contrast, CCN instruments routinely

8   activate essentially all particles into droplets at $1.01 - 1.02$.

9   We suggest laboratory work determining the extent of aerosol particle spreading variability

10   be conducted for all CFDC chambers to minimize this bias and its variability. We suggest this

11   work would (1) explore how experimental and chamber design influence the spreading effect,

12   drawing comparisons to computational fluid dynamics simulations to complement the RFR

13   statistical modeling and (2) which operational considerations (such as flow rates, inlet pressure

14   drop, etc.) maximize the probability of isokinetic injection of particles into the chamber and (3)

15   consider other freezing regimes such as depositional nucleation of ice.

1   **Acknowledgements**

2   The authors gratefully acknowledge funding from NASA grant # NNX13AO15G, NSF grant #

3   AGS-1461347, NSF grant # AGS-1339264, and DOE grant # DE-SC0014487. Z. A. Kanji and

4   R. O. David would like to acknowledge funding from SNF grant # 200021_156581. We would

5   like to thank the Storm Peak Laboratory staff for the use of their facilities to perform the

6   pressure-dependent timing experiments. We thank Paul DeMott, Jesse Kroll and the Fifth Ice

7   Nucleation workshop participants for helpful discussions.

1   **References**

2   Boose, Y., Sierau, B., García, M. I., Rodríguez, S., Alastuey, A., Linke, C., Schnaiter, M.,

3   Kupiszewski, P., Kanji, Z. A., and Lohmann, U.: Ice nucleating particles in the Saharan

4   Air Layer, Atmos. Chem. Phys. Discuss., doi:10.5194/acp-2016-192, in review, 2016.

5   Boucher, O., Randall, D., Artaxo, P., Bretherton, C., Feingold, G., Forster, P., Kerminen, V.-M.,

6   Kondo, Y., Liao, H., Lohmann, U., Rasch, P., Satheesh, S., Sherwood, S., Stevens, B.,

7   and Zhang, X.: Clouds and aerosols, in: Climate Change 2013: The Physical Science

8   Basis, Working Group I Contribution to the Fifth Assessment Report of the

9   Intergovernmental Panel on Climate Change, Cambridge, United Kingdom and New

10   York, NY, USA, 571-657, 2013.

11   Breiman, L.: Random Forests, Mach. Learn. 45, 5-32, doi: 10.1023/A:1010933404324, 2001.

12   Chou, C., Stetzer, O., Weingartner, E., Juranyi, Z., Kanji, Z. A., and Lohmann, U.: Ice nuclei

13   properties within a Saharan dust event at the Jungfraujoch in the Swiss Alps, Atmos.

14   Chem. Phys., 11, 4725-4738, 10.5194/acp-11-4725-2011, 2011.

15   DeMott, P. J., Cziczo, D. J., Prenni, A. J., Murphy, D. M., Kreidenweis, S. M., Thomson, D. S.,

16   Borys, R., and Rogers, D. C.: Measurements of the concentration and composition of

17   nuclei for cirrus formation, P. Natl. Acad. Sci. USA, 100, 14655-14660,

18   10.1073/pnas.2532677100, 2003a.

19   DeMott, P. J., Sassen, K., Poellot, M. R., Baumgardner, D., Rogers, D. C., Brooks, S. D., Prenni,

20   A. J., and Kreidenweis, S. M.: African dust aerosols as atmospheric ice nuclei, Geophys.

21   Res. Lett., 30, 10.1029/2003gl017410, 2003b.

22   DeMott, P.J., Prenni, A. J., Liu, X., Petters, M. D., Twohy, C. H., Richardson, M. S.,

23   Eidhammer, T., Kreidenweis, S. M., and Rogers, D. C.: Predicting global atmospheric ice

nuclei distributions and their impacts on climate, P. Natl. Acad. Sci. USA, 107, 11217-11222, 2010.

DeMott, P. J., Prenni, A. J., McMeeking, G. R., Sullivan, R. C., Petters, M. D., Tobo, Y., Niemand, M., Möhler, O., Snider, J. R., Wang, Z., and Kreidenweis, S. M.: Integrating laboratory and field data to quantify the immersion freezing ice nucleation activity of mineral dust particles, Atmos. Chem. Phys., 15, 393-409, doi:10.5194/acp-15-393-2015, 2015.

Fan, J., Leung, L. R., DeMott, P. J., Comstock, J. M., Singh, B., Rosenfeld, D., Tomlinson, J. M., White, A., Prather, K. A., Minnis, P., Ayers, J. K., and Min, Q.: Aerosol impacts on California winter clouds and precipitation during CalWater 2011: local pollution versus long-range transported dust, Atmos. Chem. Phys., 14, 81-101, doi:10.5194/acp-14-81-2014, 2014.

Forster, P., Ramaswamy, V., Artaxo, P., Berntsen, T., Betts, R., Fahey, D.W., Haywood, J., Lean, J., Lowe, D.C., Myhre, G. and Nganga, J.: Changes in atmospheric constituents and in radiative forcing, Chapter 2, United Kingdom: Cambridge University Press, 2007.

Garimella, S., Kristensen, T. B., Ignatius, K., Welti, A., Voigtländer, J., Kulkarni, G. R., Sagan, F., Kok, G. L., Dorsey, J., Nichman, L., Rothenberg, D. A., Rösch, M., Kirchgäßner, A. C. R., Ladkin, R., Wex, H., Wilson, T. W., Ladino, L. A., Abbatt, J. P. D., Stetzer, O., Lohmann, U., Stratmann, F., and Cziczo, D. J.: The SPectrometer for Ice Nuclei (SPIN): an instrument to investigate ice nucleation, Atmos. Meas. Tech., 9, 2781-2795, doi:10.5194/amt-9-2781-2016, 2016.

1   Hande, L. B., Engler, C., Hoose, C., and Tegen, I.: Seasonal variability of Saharan desert dust

2   and ice nucleating particles over Europe, Atmos. Chem. Phys., 15, 4389-4397,

3   doi:10.5194/acp-15-4389-2015, 2015.

4   Järvinen, E., Schnaiter, M., Mioche, G., Jourdan, O., Shcherbakov, V. N., Costa, A., Afchine, A.,

5   Kraemer, M., Heidelberg, F., Jurkat, T., Voigt, C., Schlager, H., Nichman, L., Gallagher,

6   M., Hirst, E., Schmitt, C., Bansemer, A., Heymsfield, A., Lawson, P., Tricoli, U.,

7   Pfeilsticker, K., Vochezer, P., Maehler, O., and Leisner, T.: Quasi-Spherical Ice in

8   Convective Clouds, J. Atmos. Sci., 73, 3885-3910, doi:10.1175/JAS-D-15-0365.1, 2016.

9   Koop, T., Luo, B., Tsias, A. and Peter, T.: Water activity as the determinant for homogeneous ice

10   nucleation in aqueous solutions, Nature, 406, 611-614, doi:10.1038/35020537, 2000.

11   Rogers, D. C.: Development of a continuous flow thermal gradient diffusion chamber for ice

12   nucleation studies, Atmos. Res., 22, 149-181, 1988.

13   Rogers, R. R., and Yau, M. K.: A Short Course in Cloud Physics, Third ed., International Series

14   in Natural Philosophy, Pergamon Press, Oxford, 1989.

15   Rossow, W.B. & Schiffer, R.A.: Advances in understanding clouds from ISCCP, Bull. Am.

16   Meteorol. Soc., 80, 2261-2287.

17   Stetzer, O., Baschek, B., Lüönd, F., and Lohmann, U.: The Zurich Ice Nucleation Chamber

18   (ZINC) - A new instrument to investigate atmospheric ice formation, Aerosol Sci.

19   Technol., 42, 64-74, 10.1080/02786820701787944, 2008.

20   Storelvmo, T., Hoose, C., and Eriksson, P.: Global modeling of mixed-phase clouds: The albedo

21   and lifetime effects of aerosols, J. Geophys. Res., 116, D05207,

22   doi:10.1029/2010JD014724, 2011.

1 Skrotzki, J., Connolly, P., Schnaiter, M., Saathoff, H., Mohler, O., Wagner, R., Niemand, M.,

2   Ebert, V., and Leisner, T.: The accommodation coefficient of water molecules on ice -

3   cirrus cloud studies at the AIDA simulation chamber, Atmos. Chem. Phys., 13, 4451-

4   4466, doi:10.5194/acp-13-4451-2013, 2013.

5 Tan, I. and Storelvmo, T.: Sensitivity Study on the Influence of Cloud Microphysical Parameters

6   on Mixed-Phase Cloud Thermodynamic Phase Partitioning in CAM5, J. Atmos. Sci.,

7   73(2), 709-728, doi:10.1175/jas-d-15-0152.1, 2016.

8 Tobo, Y., Prenni, A. J., DeMott, P. J., Huffman, J. A., McCluskey, C. S., Tian, G., Pöhlker, C.,

9   Pöschl, U., and Kreidenweis, S. M.: Biological aerosol particles as a key determinant of

10   ice nuclei populations in a forest ecosystem, J. Geophys. Res.-Atmos., 118, 10100-10110,

11   doi:10.1002/jgrd.50801, 2013.

12 Vergara-Temprado, J., Wilson, T.W., O'Sullivan, D., Browse, J., Pringle, K.J., Ardon-Dryer, K.,

13   Bertram, A.K., Burrows, S.M., Ceburnis, D., DeMott, P.J. and Mason, R.H.: Contribution

14   of feldspar and marine organic aerosols to global ice nucleating particle concentrations,

15   Atmos. Chem. Phys., Discuss., doi:10.5194/acp-2016-822, 2016.

17 Xie, S., Liu, X., Zhao, C., and Zhang, Y.: Sensitivity of CAM5-Simulated Arctic Clouds and

18   Radiation to Ice Nucleation Parameterization, J. Climate, 26, 5981-5999, doi:

19   10.1175/JCLI-D-12-00517.1, 2013.

Feature Rank	Feature Name
1	Lamina Saturation at TC3
2	Average ΔT between Warm and Cold Wall
3	Lamina Saturation at TC4
4	Warm Wall H0 On/Off Time
5	Lamina Saturation at TC1
6	Lamina Saturation at TC11
7	Average Warm Wall Temperature Spread
8	Lamina Saturation at TC5
9	Average Warm Wall Temperature Difference from Set Point
10	Total Volume Flow

2   Table 1: List of the ten most important features from the RFR. TC corresponds to Thermocouple

3   and H to heater (supplemental heating is used to maintain wall isothermality in the SPIN

4   chamber) where numbers correspond to locations described in Garimella et al. (2016). Lamina

5   saturation is calculated at specific locations using temperature measurements and assuming walls

6   exist at ice saturation per the method outlined in Garimella et al. (2016). The features are

7   predominantly located in the top and middle sections of the chamber.
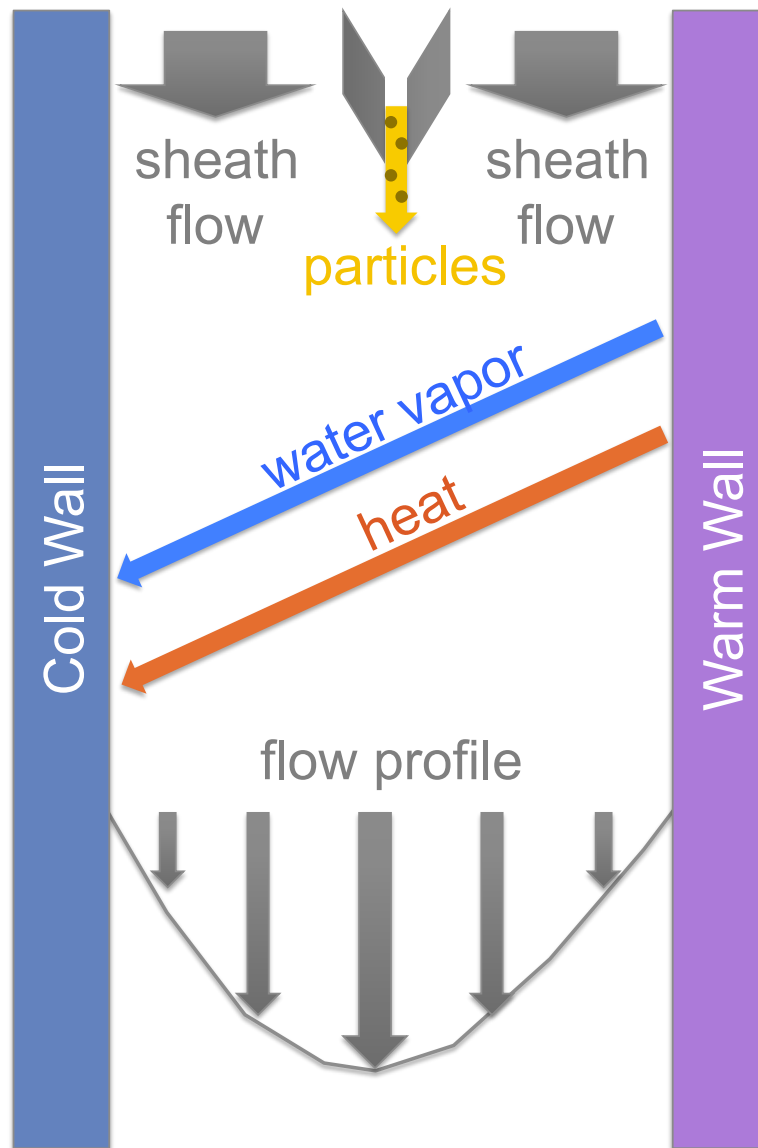
Figure 1: Schematic representation of an idealized CFDC. A particle-laden flow is passed

between two ice-coated walls that are held at different temperatures below 0ºC. This results in

water vapor and heat diffusing from the warm to the cold wall. Supersaturation, with a maximum

near the centerline, results from the non-linear relationship of water vapor saturation with respect

to temperature. Sheath flows along each wall are meant to isolate particles to a central lamina at

or near the supersaturation maximum, which also theoretically restricts the temperature and

superstation to which they are exposed.
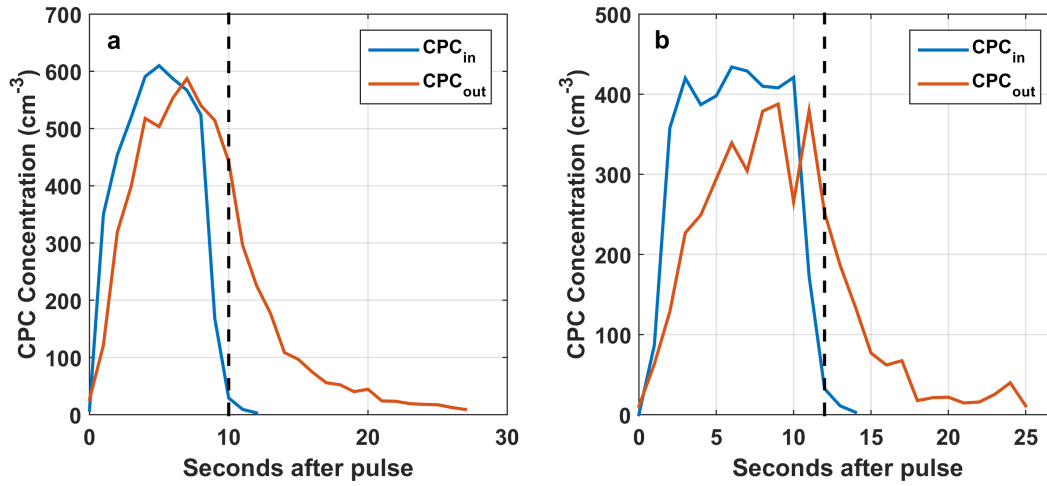
Figure 2. Particle concentration as a function of time for particle pulse experiments using ZINC. The blue traces are the counts measured at the entrance of the chamber (CPC_{in}) while the red traces are the concentrations at the output (CPC_{out}). Both experiments were conducted at -40° C with Panel a at 102% RH and Panel b at 110% RH, both with respect to liquid water. Particles in the red trace occurring after the vertical dashed line are outside the initial pulse duration and are inferred to have moved out of the lamina. The ratio of particles within the pulse time at the outlet versus the total particles were 78 and 76% for Panels a and b, respectively.
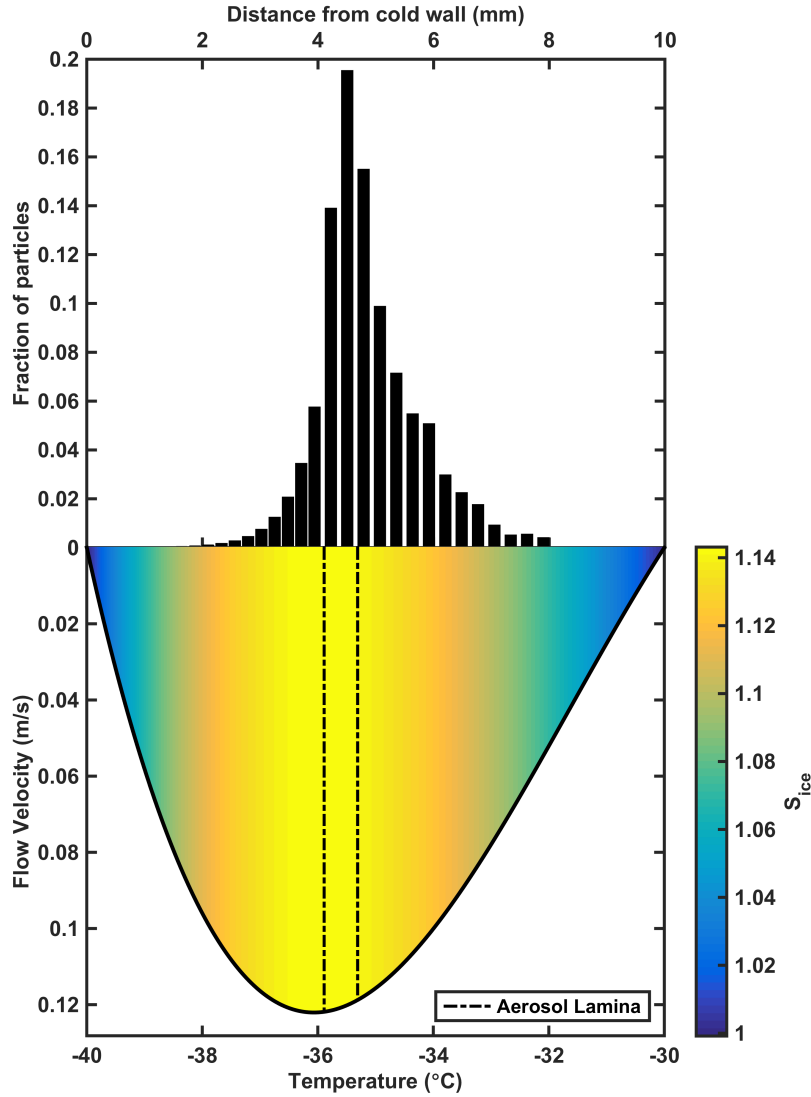
Figure 3. Measured particle distribution across the chamber in the SPIN CFDC (Top; see text for details) corresponding to the velocity profile and S_{ice} as a function of temperature across the chamber (Bottom). The dash-dot lines show the location of particles if they were constrained to the theoretical aerosol lamina. Note that while the peak particle concentration correctly occurs within the lamina, some particles have migrated into the sheath and are therefore exposed to higher and lower temperatures and supersaturation lower than the maximum.
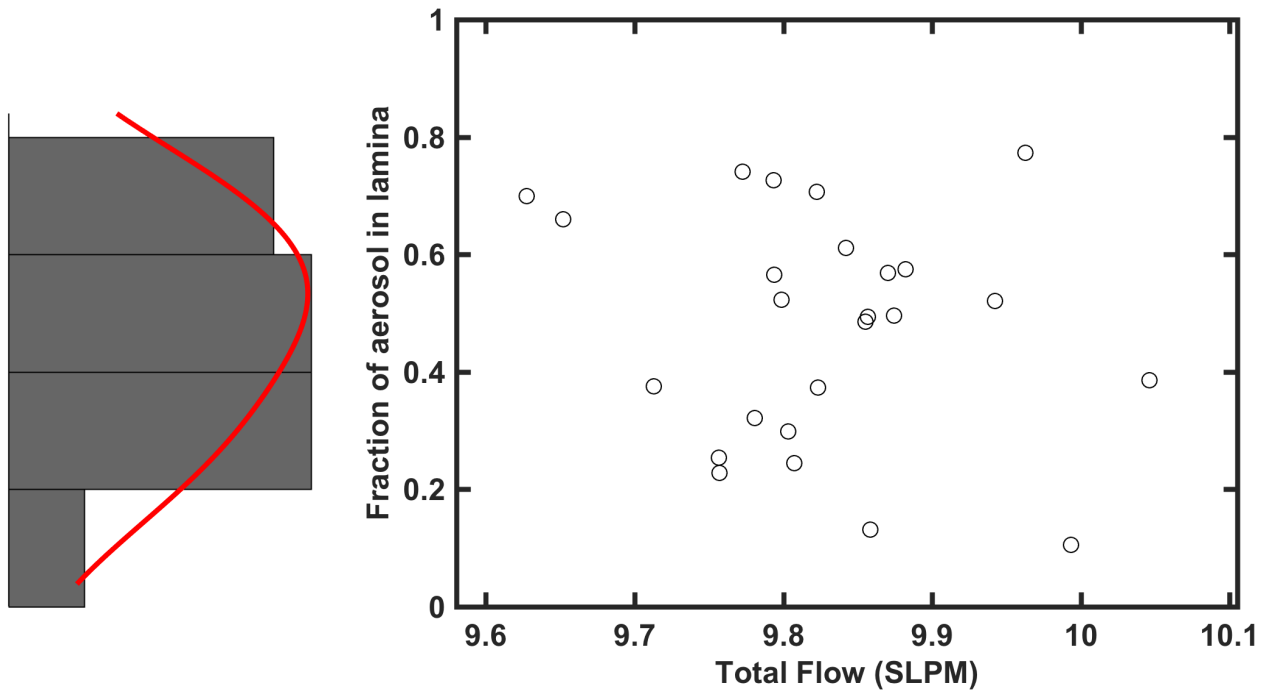
2 Figure 4. Measured f_{lam} as a function of total flow in SPIN at 20° C, varied around a nominal

3 value of 9.8 slpm. In the ideal case, where all particles are constrained with the dash-dot lines in

4 Figure 2, data points should form a horizontal line at 1.0. This figure illustrates that the ideal

5 condition is not realized and that even within a few % of the nominal total flow of 9.8 lpm, the

6 fraction of particles in the lamina is not predictable. The histogram on the left is a distribution of

7 f_{lam} with the corresponding kernel density estimate shown in red.
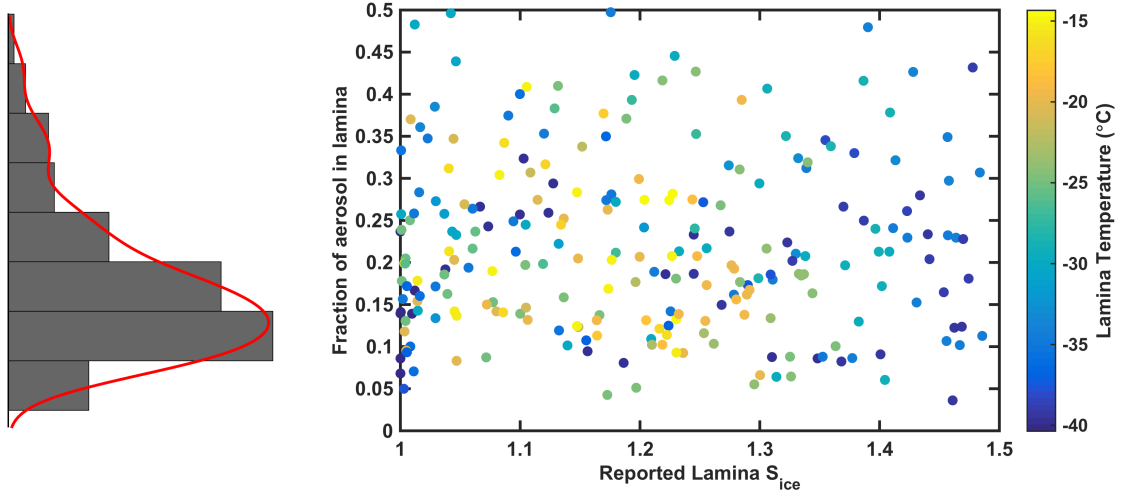
2   Figure 5. Measured f_{lam} as a function of S_{ice} in the aerosol lamina in SPIN. Temperature for

3   each data point is noted by the color bar. The histogram on the left is the distribution of f_{lam}

4   from the measurements with the corresponding kernel density estimate shown in red.
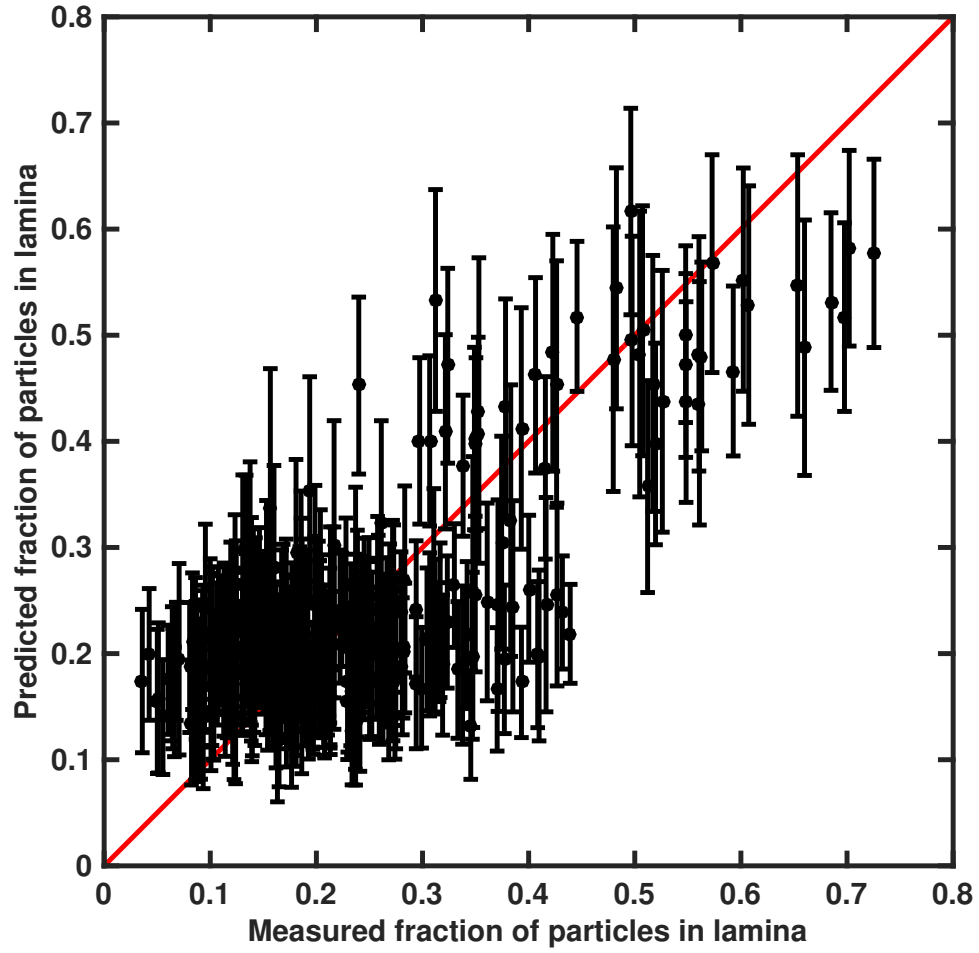
2 Figure 6. Random forest regression prediction versus measured f_{lam} using the 65 SPIN variables

3 determined by the algorithm to be most important (see text for details). Data points are the mean

4 value predicted and error bars correspond to the standard deviation of the predictions by the

5 random forest. A one-to-one line is shown in red.
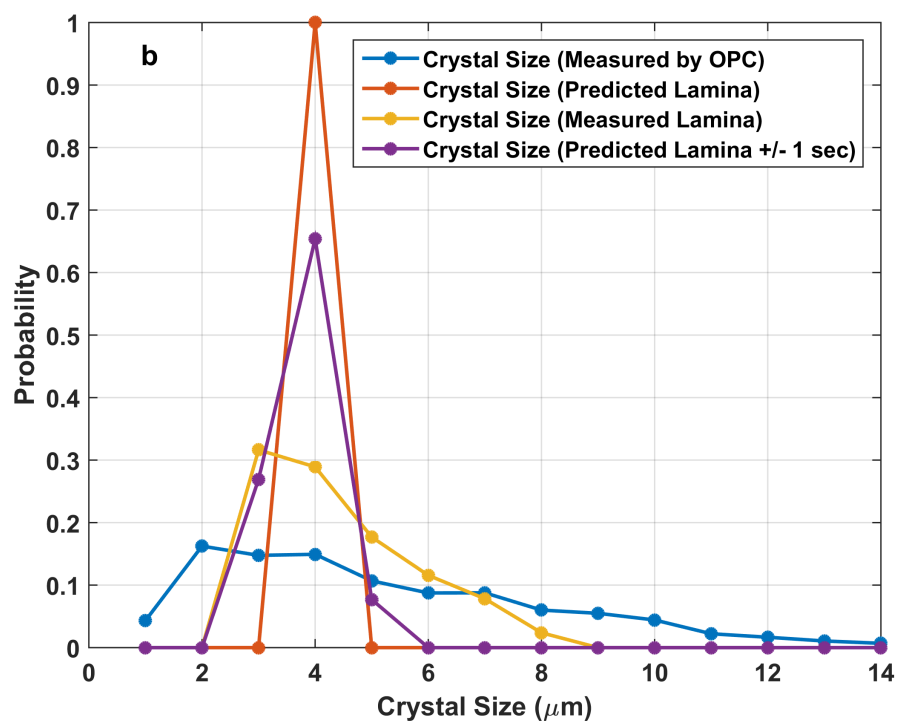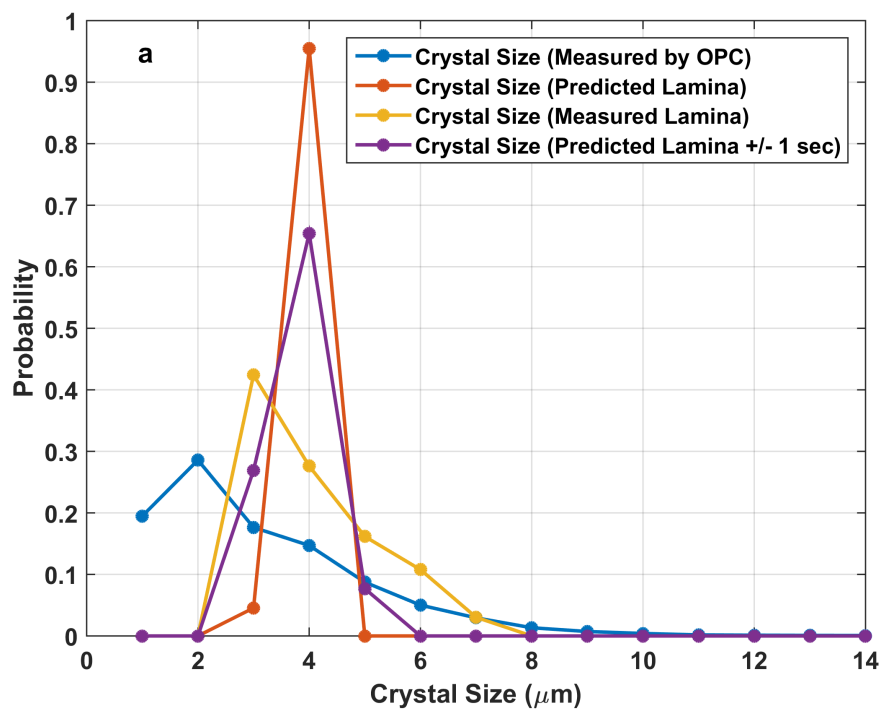
3   Figure 7. Probability histogram of ice crystal diameter. Both experiments were conducted at -

4   40°C with Panel a at 102% RH and Panel b at 110% RH, both with respect to liquid water. In the

1   predicted case all particles are assumed to remain within the lamina, nucleate ice and grow to the

2   same final size (red). The ice crystal size distribution becomes broader if particles are allowed to

3   exist in the chamber for 1 second shorter or longer than predicted (purple). Ice crystal size

4   predictions using the spreading time indicated in Figure 2 results in the yellow histogram. Note

5   that the ice crystal size predictions using the measured spreading time (yellow) most closely

6   matches the measured ice crystal size distribution (blue) from the ZINC OPC.
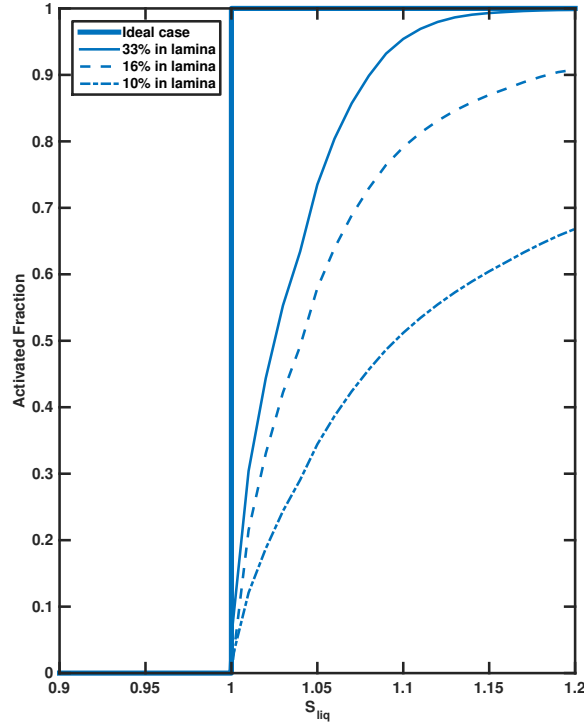
2   Figure 8. Fraction of particles that activate as a function of saturation with respect to liquid

3   water. All particles are assumed to be perfect immersion INPs which activate as ice crystals

4   when exposed to water saturation (S_{liq}=1). In the ideal case, where all particles are constrained

5   within the lamina (f_{lam} 100%; all particles exist within the dash-dot lines in Figure 2), all

6   nucleation occurs at a CFDC saturation of S_{liq}=1 (bold solid line). The other three curves

7   correspond to increasingly less ideal behavior (i.e., increasingly fewer particles in the lamina and

8   existing farther from the centerline), corresponding to f_{lam} falling from 33 to 10%. In these cases

9   an increasingly higher maximum CFDC saturation is required so that the particles farthest from

10   the centerline experience S_{liq}=1.
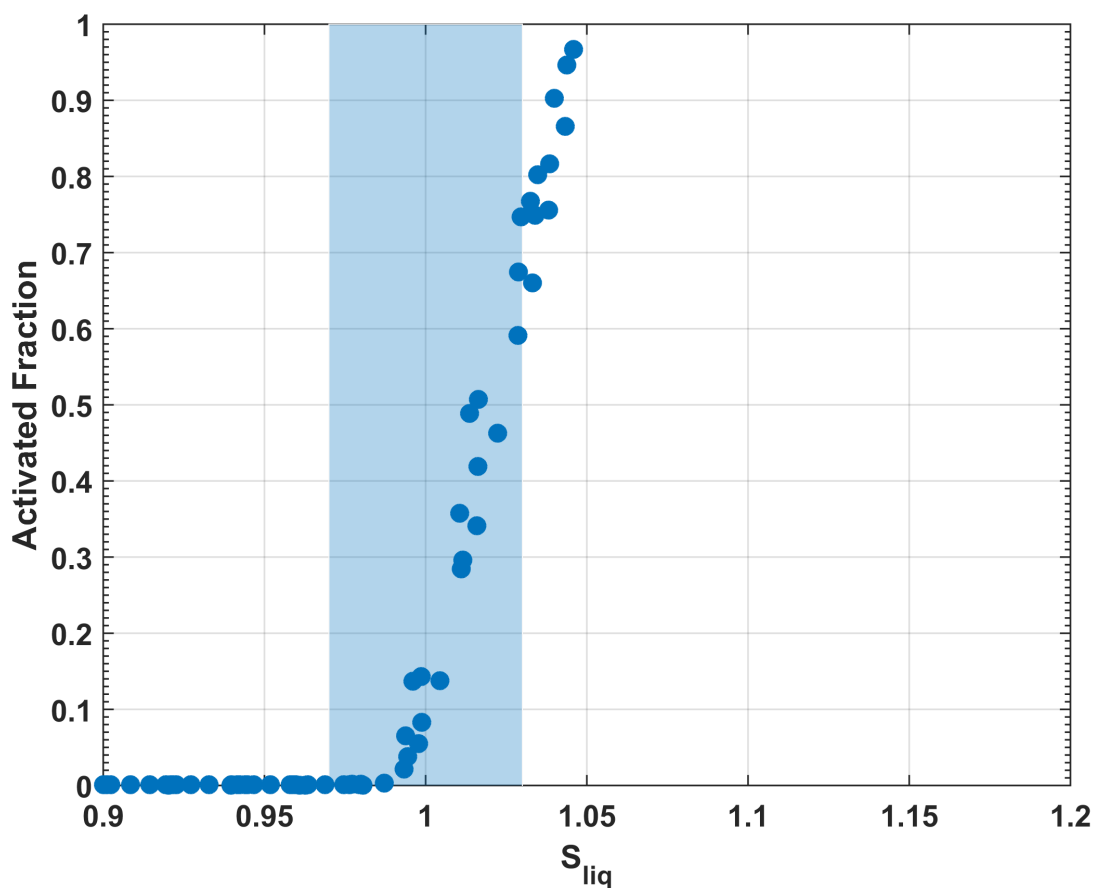
2 Figure 9. Fraction of 400 nm (dry diameter) NH_4NO_3 particles freezing homogenously as a

3 function of S_{liq} in ZINC at -40 °C. For these conditions particles should freeze at $S_{liq} \sim 0.99$

4 (Koop et al., 2000). Shaded region indicates the range and uncertainty of S_{liq} that the aerosol in

5 the lamina are exposed to.
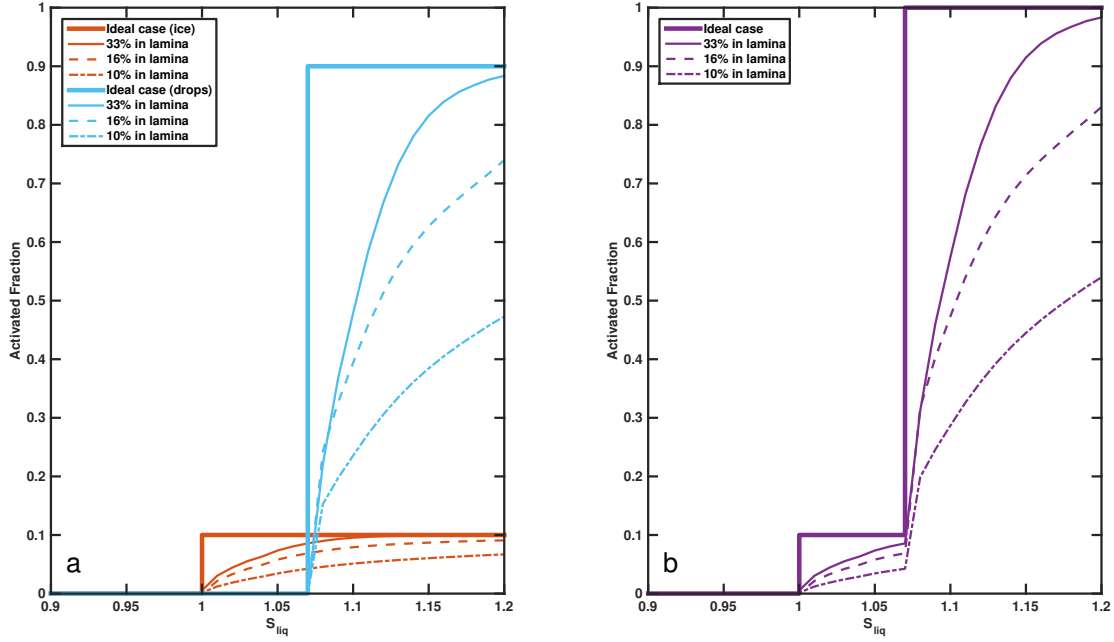
2   Figure 10. Fraction of particles that activate as a function of saturation with respect to liquid

3   water. Unlike Figure 8, where all particles are assumed to be perfect immersion INPs which

4   activate as ice crystals when exposed to water saturation (S_{liq}=1), only 10% of particles are

5   assumed to be perfect immersion INPs. In the ideal case where all particles are constrained

6   within the lamina (f_{lam} 100%; all particles exist within the dash-dot lines in Figure 2), 10% of

7   particles nucleate ice at a CFDC saturation of S_{liq}=1 (panel a, bold red line). The remaining 90%

8   of particles are assumed to be perfect CCN that activate at $S_{liq} = 1$. Droplets only survive the

9   evaporation region of the chamber at $S_{liq} > 1.07$ (corresponding to a "droplet breakthrough"

10   point; bold blue line, see text and Garimella et al. (2016) for details). The other three curves

11   correspond to the increasingly less ideal behavior presented in Figure 8, with f_{lam} falling from

12   33 to 10%. In these cases, an increasingly higher maximum CFDC saturation is required so that

13   the particles farthest from the centerline experience S_{liq}=1 and 1.07. The resulting activation

14   curves if droplets and ice crystals are indistinguishable, as is the case for an OPC, (i.e., a

15   composite of the red and blue traces in panel a) is shown in panel b.